

Microporosity of Bicontinuous Nanoporous Polymeric Materials, Characterized with Restricted Diffusion

V. Challa,[†] K. Kuta,[‡] S. Lopina,[†] H. M. Cheung,[†] and E. von Meerwall*,^{‡,§}

Departments of Chemical Engineering, Physics, and Polymer Science, The University of Akron,
Akron, Ohio 44325-3906

Received August 27, 2002. In Final Form: January 10, 2003

The ¹H NMR pulsed-gradient spin-echo method has been used to study the self-diffusion *D* of the mobile fractions in polymerized bicontinuous microemulsions formed with methyl methacrylate and hydroxyethyl methacrylate, cross-linked with ethylene glycol dimethacrylate, and water containing 10% sodium dodecyl sulfate as surfactant. Measurements were made at 50.5 °C over the bicontinuous range (30–96 wt % water) at diffusion times between 8 and 1000 ms. In addition to the signal from the nondiffusing glassy phase, two distinct components are observed differing in *D* by 2 orders of magnitude, with an intensity ratio monotonic in water content. Both *D* values depend weakly on diffusion time, but *D* attributed to free water increases with water content, whereas *D* attributed to surfactant decreases with water content in the bicontinuous region. This may be due to a size reduction in the surfactant micelles in samples containing less aqueous phase. Assuming free diffusion of water in the open pores, we extract from the data the reduced permeabilities (i.e., detour and tortuosity), discuss the origin of the slow-*D* component as surfactant undergoing surface-exchange with the network, and derive an upper limit on the pore size on the order of 1 μm near the midpoint of the bicontinuous concentration domain, in keeping with evidence from SEM imaging; a pore size distribution derived from freezing point depression attests to a large aspect ratio of the porosities.

I. Introduction

Microemulsions composed of biocompatible components are known under certain conditions to be useful in medical and pharmacological applications, for example, as vehicles for the delivery of therapeutic agents or for the protective encapsulation of living cells. If one phase of the emulsion is polymerized and has a glass transition temperature higher than body temperature, subcutaneous implantation or injection may be envisioned. To provide mechanical robustness and resistance to erosion, the glassy phase should be monolithic, continuous over the specimen; to permit controlled and locally targeted drug delivery, the interpenetrating fluid phase must also be continuous and have appropriately high macroscopic permeability. Minimal immunogenic response is a firm prerequisite determining materials selection.

Nanoporous polymer materials meeting these requirements may be obtained by preparing bicontinuous microemulsions at least one of whose components is subsequently polymerized. The microemulsions typically contain an aqueous component and oil stabilized by a surfactant, perhaps with the addition of a cosurfactant. While a microemulsion does not act as a true template for polymerization, many nanostructural features of the precursor microemulsion can be preserved.

The polymerization of microemulsions in general has been well studied. The preparation of porous polymeric materials by the polymerization of monomer-containing microemulsions has been a particularly active area of inquiry.^{1–4} The relationship between the precursor mi-

croemulsion nanostructure and the morphology of the nanoporous polymeric solids has been investigated.^{5,6} Numerous monomer species have been studied.^{7–10} The present work reports the results of proton nuclear magnetic relaxation and time-resolved self-diffusion experiments on a bicontinuous nanoporous polymer based on a glassy cross-linked network composed of methyl methacrylate and hydroxyethyl methacrylate, containing in its open pores between 30 and 96 wt % of a 10% aqueous solution of sodium dodecyl sulfate acting as surfactant. The results establish the highly concentration-dependent long-range permeability of the glassy structure to the liquid phase, semiquantitatively confirm the mean size of the open pores on the order of 1 μm, and detect evidence of exchange of surfactant molecules with the surface of the network. Preliminary oral reports of this work have been presented.^{11,12}

PGSE NMR has been used by Chew et al.¹³ to characterize a similar microemulsion using a polymerizable surfactant instead of sodium dodecyl sulfate. They reported a similar trend in reduced water diffusion coefficient for both unpolymerized and polymerized microemulsions over the water content range from 27% to 45% water.

(4) Haque, E.; Qutubuddin, S. *J. Polym. Sci., Polym. Lett. Ed.* **1990**, *26*, 429.

(5) Palani Raj, W. R.; Sasthav, M.; Cheung, H. M. *J. Appl. Polym. Sci.* **1993**, *47*, 499.

(6) Sasthav, M.; Cheung, H. M. *Langmuir* **1991**, *7*, 1378.

(7) Chieng, T. H.; Gan, L. M.; Chew, C. H.; Ng, S. C. *Polymer* **1995**, *36* (10), 1941.

(8) Gan, L. M.; Chieng, T. H.; Chew, C. H.; Ng, S. C. *Langmuir* **1994**, *10* (11), 4022.

(9) Palani Raj, W. R.; Sasthav, M.; Cheung, H. M. *Langmuir* **1991**, *7*, 2586.

(10) Palani Raj, W. R.; Sasthav, M.; Cheung, H. M. *Langmuir* **1992**, *8*, 1931.

(11) Kuta, K.; Challa, V.; Cheung, H. M.; Lopina, S. T.; von Meerwall, E. D. *Bull. Am. Phys. Soc.* **2000**, *45*, 13.

(12) von Meerwall, E. D.; Kuta, K.; Challa, V.; Lopina, S. T.; Cheung, H. M. *Bull. Am. Phys. Soc.* **2001**, *46*, 321.

(13) Chew, C. H.; Gan, L. M.; Ong, L. H.; Zhang, K.; Li, T. D.; Loh, T. P.; MacDonald, P. M. *Langmuir* **1997**, *13*, 2917.

[†] Department of Chemical Engineering.

[‡] Department of Physics.

[§] Department of Polymer Science.

(1) Stoffer, J. O.; Bone, T. J. *J. Dispersion Sci. Technol.* **1980**, *1*, 393.

(2) Menger, F. M.; Tsuno, T.; Hammond, G. S. *J. Am. Chem. Soc.* **1990**, *112*, 1263.

(3) Palani Raj, W. R.; Sasthav, M.; Cheung, H. M. *Polymer* **1995**, *36* (13), 2637.

They found that the reduced diffusion coefficient increased over that range but was higher for the unpolymerized microemulsions. We have studied time-resolved diffusion, over a wider water content range (30% to 96% aqueous) and have found evidence of a second diffusing species which we identify as surfactant micelles.

II. Experiment

The starting materials for the present study were methyl methacrylate (MMA) and hydroxy ethyl methacrylate (HEMA) monomers mixed in the proportion 1:3. Ethylene glycol dimethacrylate (EDGMA) was used as cross-linking agent at a concentration of 4 wt % of the monomer. AIBN, azobisisobutyronitrile, was added as polymerization initiator at a concentration of 0.002 wt %. A 10 wt % aqueous solution of sodium dodecyl sulfate (SDS) was prepared and added to constitute between 30% and 96% of the sample by weight. Eleven samples covered this concentration range known to span the full bicontinuous two-phase domain. All chemicals were obtained from Aldrich and were used as received.

Aliquots of these mixtures were placed into 7 mm o.d. NMR sample tubes, equilibrated for 24 h, purged with dry N_2 gas, and thermally polymerized at 55 °C for 3 h. While we did not make quantitative conversion measurements, these conditions appear to lead to nearly complete conversion of the monomers. The polymerized samples have little or no monomer odor. The sample tubes were hermetically sealed before use in NMR experiments after a room-temperature storage time of at least 1 week.

Pulsed-Gradient NMR Diffusion Measurements and Interpretation. Self-diffusion measurements in the bicontinuous nanoporous materials were performed using the pulsed-gradient spin-echo (PGSE) method, which is based on pulsed nuclear magnetic resonance (NMR). Our implementation of the high-gradient, nonspectroscopic variant of this method has been described in its early form in previous publications^{14–18} and has since been continuously refined and upgraded.^{19,20} The equipment is based on a stable current-regulated, high-impedance iron-core magnet and a 33 MHz modified Spin-Lock CPS-2 spectrometer. Measurements of the proton spin-echo amplitude were performed at 50.5 °C, the temperature being controlled within 0.2 °C with a steady stream of heated air. The radio frequency (rf) pulse programs used were the principal spin-echo sequence $90^\circ - \tau - 180^\circ - \tau$ -echo for diffusion times $8 \text{ ms} \leq \tau \leq 30 \text{ ms}$ and the stimulated echo sequence $90^\circ - \tau_1 - 90^\circ - (\tau_2 - \tau_1) - 90^\circ - \tau_1$ -echo for diffusion times $100 \text{ ms} \leq \tau_2 \leq 1000 \text{ ms}$. For the latter cases, τ_1 was fixed at 12 ms. The rather conservative lower limit for the diffusion time was determined by the need to avoid even small residual-gradient effects¹⁶ to permit precise comparisons, while the upper limit was set by the finite spin relaxation times in the aqueous phase.

A pair of magnetic field gradient pulses was applied in conjunction with the rf pulses, such that the diffusion time $t = \tau$ and $t = \tau_2$ for the principal echo sequence and the stimulated echo sequence, respectively. The gradient pulses, applied to the sample using gradient coils in the high-uniformity Zupančič–Pirš configuration,²¹ had a magnitude G of 671 G/cm at short diffusion times and 152 G/cm above 50 ms, using a common calibration. The duration δ of the gradient pulses was varied in 8 to 20 increments from zero until the echo was attenuated to below 3% of its original height; the maximal value of δ was 4 ms. A steady gradient $G_0 \approx 0.3 \text{ G/cm}$ was also applied for convenience in data collection; it has no effect on echo attenuation during the

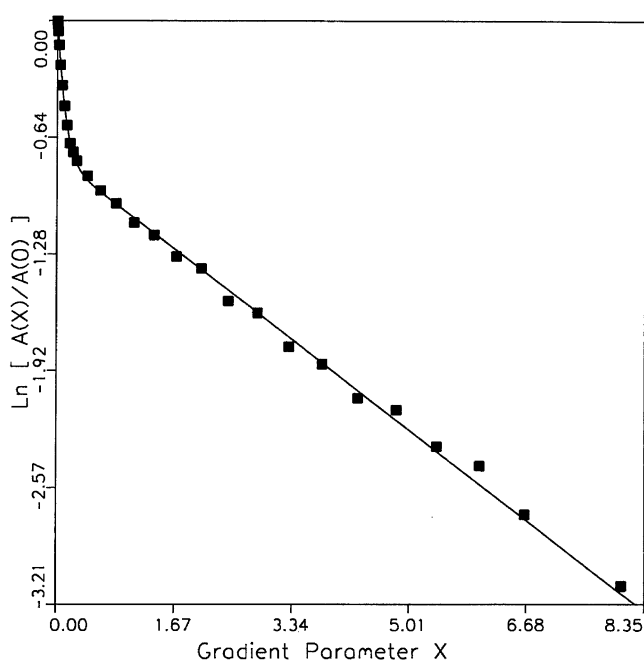


Figure 1. Logarithmic diffusional NMR spin-echo attenuation at a diffusion time of 15 ms in a polymerized microemulsion with 40% aqueous content. The abscissa variable X has units of $10^{-3} \text{ G}^2 \text{ s}^3 \text{ cm}^{-2}$. Error bars are approximately the size of symbols denoting measured echo attenuation data; the line represents a successful three-parameter fit of eq 1. Diffusion rates of surfactant micelles (slow) and water (fast) differ by a factor of 40. The echo signal from the glassy network is not observable at any of our PGSE settings due to its short T_2 .

period between the second and third 90° pulses in the stimulated echo sequence, where spin relaxation is longitudinal. For the PGSE work, the spectrometer was operated in single-sideband mode, -3 kHz off resonance, and the signal was demodulated using rf phase-sensitive detection. The echo amplitude recorded was the magnitude Fourier transform integrated across the echo peak with an rms correction for the noise integral. Between 5 and 15 signals were acquired and averaged for each setting of δ . The echo amplitudes A versus δ were analyzed using an off-line computer code (DIFUS5²² in its current PC version) which fitted to the data the expression²³ appropriate for two components diffusing at different rates:

$$A(\delta)/A(\delta=0) = f_{\text{fast}} \exp(-\gamma^2 D_{\text{fast}} X) + (1 - f_{\text{fast}}) \exp(-\gamma^2 D_{\text{slow}} X) \quad (1)$$

For the principal echo sequence the combined gradient parameter X takes the form $X = G^2 \delta^2 (\tau - \delta/3)$ with additional minor correction terms²³ in GG_0 . The gyromagnetic ratio of the nuclei (here protons) is denoted by the symbol γ . The three adjustable parameters in eq 1 are the two diffusion coefficients D_{fast} and D_{slow} and the relative intensity f_{fast} .

In most instances, two diffusing components were observed and cleanly resolvable; on the basis of both their rates and relative echo intensities, their identification with free water and surfactant micelles was elementary. A typical echo attenuation plot is shown in Figure 1 together with the fit of eq 1. Diffusion measurements for a sample of 20% aqueous content, below the lower limit of the bicontinuous domain, could not be performed due to the short T_2 relaxation time for both components. At 30% aqueous content water diffusion was measurable, but the surfactant echo was too small even at short diffusion times to permit attenuation measurements. At a diffusion time of 1000 ms, quantitative extraction of the fast rate was reliable only above 80% aqueous content, and no measurements of the slow

(14) von Meerwall, E.; Burgan, R. D.; Ferguson, R. D. *J. Magn. Reson.* **1979**, *34*, 339.

(15) von Meerwall; Ferguson, R. D. *J. Appl. Polym. Sci.* **1979**, *23*, 877.

(16) von Meerwall, E.; Kamat, M. *J. Magn. Reson.* **1989**, *83*, 309.

(17) Iannacchione, G.; von Meerwall, E. *J. Polym. Sci., Polym. Phys. Ed.* **1993**, *31*, 1029.

(18) Pacanovsky, J.; Kelley, F. N.; von Meerwall, E. *J. Polym. Sci., B: Polym. Phys.* **1994**, *32*, 1339.

(19) von Meerwall, E.; Beckman, S.; Jang, J.; Mattice, W. L. *J. Chem. Phys.* **1998**, *108*, 4299.

(20) von Meerwall, E.; Feick, E. J.; Ozisik, R.; Wattice, W. L. *J. Chem. Phys.* **1999**, *111*, 750.

(21) Zupančič, I.; Pirš, J. *J. Phys. (London)* **1976**, *E9*, 79.

(22) von Meerwall, E.; Ferguson, R. D. *Comput. Phys. Commun.* **1981**, *21*, 421.

(23) Stejskal, E. O.; Tanner, J. E. *J. Chem. Phys.* **1965**, *42*, 288.

rate were possible in any sample. Independent measurements of the transverse relaxation rate spectrum showed that the glassy network invariably had a transverse relaxation time $T_2 < 1$ ms, and thus its echo component was not detectable in our PGSE experiments even at our shortest diffusion times of 8 ms, corresponding to $2\tau = 16$ ms.

The effects of internal magnetic field gradients on transverse relaxation and PGSE diffusion experiments on the fluid components in porous media have been studied extensively.^{24,25} The attendant spin dephasing is most pronounced in systems in which the fluid and solid phases have significant differences in magnetic susceptibility, in the presence of embedded paramagnetic impurities, in the limit of small pore sizes, and at large diffusion times. In PGSE experiments, such effects can be detected by an unorthodox dependence of the echo attenuation on instrument settings and pulse sequences, that is, nonadherence to a master curve implied by eq 1 with X as defined. Various checks performed to elicit a signature of internal-gradient effects, or of a loss of transverse magnetization from other barrier-related causes,^{26,27} failed to detect significant differences. We therefore regard our restricted diffusion results as unaffected by artifacts.

Restricted diffusion is evidenced in PGSE measurements by an explicit time dependence of the (apparent) diffusion coefficient D_{app} .^{28–30} Under suitable conditions adhered to here, D_{app} at a given diffusion time t may be confidently extracted from echo attenuation data using eq 1. A closed exact expression for $D_{app}(t)$ is not available even for the simplest geometries, but useful largely model-independent information can still be extracted from corresponding data. In the absence of complex diffusant–surface interactions,^{26,31} measurements at short times find most of the diffusant nearly free, that is, between encounters with restraining solids or membranes, so that its diffusion rate D_0 resembles that in the neat liquid. At long times the diffusion rate will approach a lower asymptote D_∞ characteristic either of multiple attempts required to penetrate each in a structure of semipermeable membranes or else of multiple encounters with impenetrable but circumnavigable solids (as in the present work). The dimensionless reduced permeability,²⁹

$$p = [D_0/D_\infty - 1]^{-1} \quad (2)$$

originally intended for structures containing membranes, may also serve to characterize the long-range detour and tortuosity factors involved in traversing open-cell networks. If the barrier spacings are regular, or at least have a narrow distribution about a single modal value, an estimate of this mean spacing $\langle a \rangle$ may be obtained from the time t^* at which D has reached the logarithmic midpoint between D_0 and D_∞ . Using the Einstein relation for random walks projected on one dimension, one finds semiquantitatively^{28,29}

$$\langle a \rangle \approx [3D_0 t^*]^{0.5} \quad (3)$$

If at the shortest accessible diffusion time D_{app} is already substantially reduced below D_0 (e.g., as measured in the neat liquid) and is approaching D_∞ , only an upper limit for $\langle a \rangle$ will be extractable from the data. Conversely, if the asymptotic limit $D_{app}(t) = D_\infty > 0$ is inferred from measurements at times $t \gg t^*$, and hence for rms diffusion distances greatly in excess of $\langle a \rangle$, it may be confidently concluded that the specimen is macroscopically permeable.

Scanning Electron Microscopy. A JEOL JSM 53101 scanning electron microscope was used to study the morphology of the polymer samples. Samples were air-dried for at least 1

week. A small fragment of each sample was then mounted on a sample-mount and sputter coated for about 80 s with silver using a Polaron E5400 sputter coater. The sample was then mounted in the scanning electron microscope, and the morphology of the sample was studied at the desired magnification.

Freezing Point Depression. The freezing point of the water present in the nanoporous material is depressed due to the high curvature of the interfaces present. This freezing depression can be used as a probe of the pore size distribution.^{32,33}

$$T_0 - T_m = \frac{2\gamma T_0}{\rho_w \lambda R} \quad (4)$$

Here T_0 is the normal melting point, T_m is the observed melting point, γ is the interfacial tension, ρ_w is the density, λ is the heat of fusion, and R is the pore radius. The pore size distribution is obtained by measuring the heat flow as a function of temperature and using the above relation. This technique has been applied by our group³⁴ and others^{35,36} in the characterization of nanoporous materials produced by microemulsion polymerization. A DuPont Instruments –910 differential scanning calorimeter system along with a DuPont Thermal Analyst 2100 system was used to measure the enthalpy flow, as the sample was thawed. A few milligrams of the sample were weighed and then hermetically sealed in a high-pressure pan. The sample was frozen in dry ice for 24 h in order to freeze all the water in the pores. The sample was then placed in the DSC cell and allowed to equilibrate at -40 °C, after which it was heated at a ramp rate of 1 °C/min until -15 °C. The sample was then held isothermally for 5 min at -15 °C, after which a ramp rate of 0.25 °C/min was applied until a temperature of 4 °C was reached. The run was then terminated, and a plot of the enthalpy flow against melting temperature was obtained. These data were then converted to a plot of pore size versus pore volume using eq 4.

III. Results and Discussion

Scanning Electron Microscopy. Scanning electron microscopy (SEM) was used to examine the gross morphology of the polymer monoliths. Since it is necessary to dry and fracture the samples prior to examining them under SEM, the morphology observed is not the same as that of the native material. There are significant morphological changes associated with drying in such highly hydrated, nanoporous materials. However, the SEM images do give a good indication of the gross morphology, that is, whether the structure was open or closed cell. Parts A and B of Figure 2 show the morphology of the 60% and 80% aqueous samples, respectively. There is evident porosity in each, but the SEM for the 80% aqueous sample shows evidence of possible agglomerated particles. As the aqueous content of the system increases, the precursor microemulsion transitions from a bicontinuous to an oil-in-water structure and the resulting polymeric materials shift from nanoporous solids to disperse particles.

Pore Size Distribution from Freezing Point Depression. The pore size distributions for aqueous contents from 60% to 90% obtained from freezing point depression (FPD) are shown in Figure 3. The majority of the pore volume lies between 100 and 200 Å in radius. This value is similar to our observations in numerous other nanoporous polymeric materials derived from microemulsion polymerization. It is worthwhile to point out, however,

(24) Hürlimann, M. *J. Magn. Reson.* **1998**, *131*, 232 and references therein.

(25) Seland, J. G.; Sørland, G. H.; Zick, K.; Havskold, Bj. *J. Magn. Reson.* **2000**, *146*, 14.

(26) Snaar, J. E. M.; Van As, H. *J. Magn. Reson. A* **1993**, *102*, 318.

(27) Coy, A.; Callaghan, P. T. *J. Chem. Phys.* **1994**, *101*, 4599.

(28) von Meerwall, E.; Ferguson, R. D. *J. Chem. Phys.* **1981**, *74*, 6956.

(29) von Meerwall, E.; Shook, D.; Min, K. J.; Kelley, F. N. *J. Appl. Phys.* **1984**, *56*, 2444 and references therein.

(30) Appel, M.; Fleischer, G.; Kärger, J.; Dieng, A. C.; Riess, G. *Macromolecules* **1995**, *28*, 2345.

(31) Park, I.-A.; MacElroy, J. M. D. *Mol. Simul.* **1989**, *2*, 105.

(32) Brun, M.; Lallemand, A.; Quinson, J. F.; Eyraud, C. *Thermochim. Acta* **1977**, *21*, 59.

(33) Enustun, B. V.; Senturk, H. S.; Yurdakul, O. *J. Colloid Interface Sci.* **1978**, *65* (3), 509.

(34) Sasthav, M.; Palani Raj, W. R.; Cheung, H. M. *J. Colloid Interface Sci.* **1992**, *152* (2), 376–385.

(35) Liu, J.; Gan, L. M.; Chew, C. H.; Teo, W. K.; Gan, L. H. *Langmuir* **1997**, *13* (24), 6421–6426.

(36) Chew, C. H.; Li, T. D.; Gan, L. H.; Quek, C. H.; Gan, L. M. *Langmuir* **1998**, *14* (21), 6068–6076.

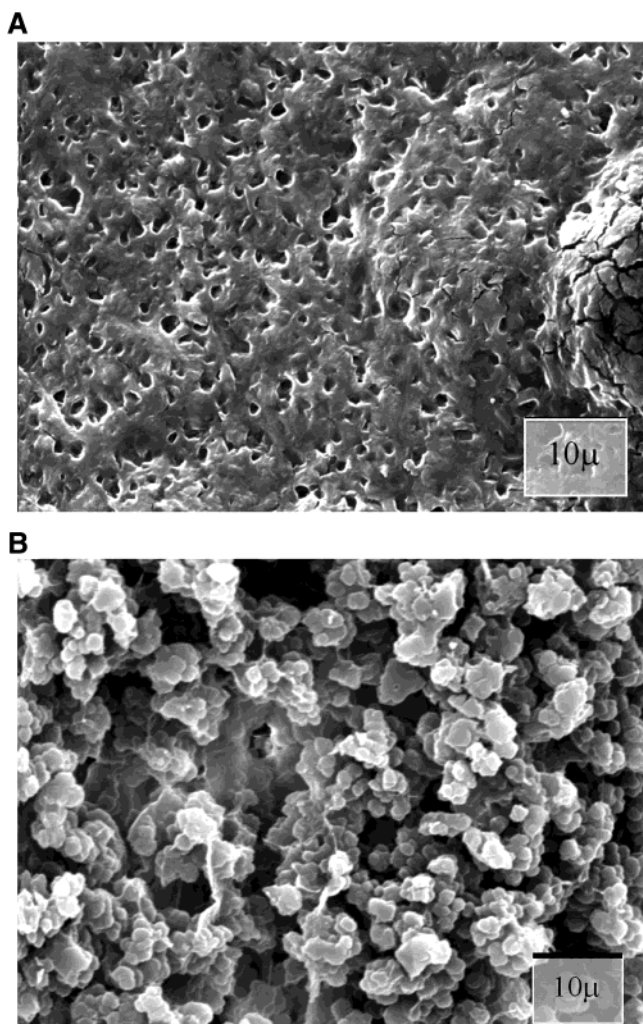


Figure 2. (A) Representative SEM image of polymer monoliths in bicontinuous composites containing (before drying) aqueous phase in the amounts of 60%, indicating porosity on the micrometer scale and suggesting particle agglomeration at the higher aqueous content. (B) Representative SEM image of polymer monoliths in bicontinuous composites containing (before drying) aqueous phase in the amounts of 80%, indicating porosity on the micrometer scale and suggesting particle agglomeration at the higher aqueous content.

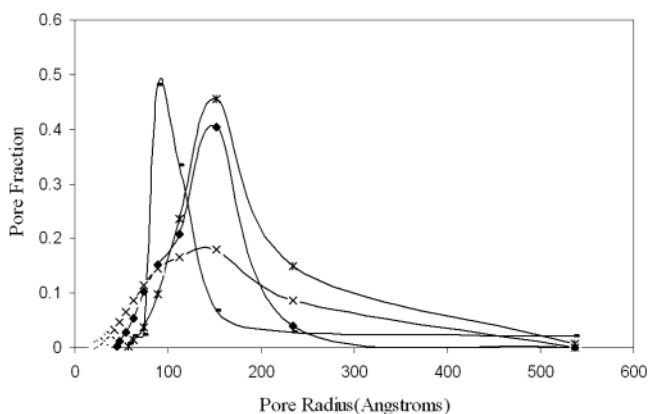


Figure 3. Pore size distribution in three bicontinuous specimens at four values of aqueous content [60% (◆); 70% (●); 80% (×); 90% (*)] obtained from freezing point depression (FDP) experiments by using eq 4.

that this dimension is not directly comparable to the pore size obtainable from partially restricted diffusion of a liquid component, which is typically much larger, as will be

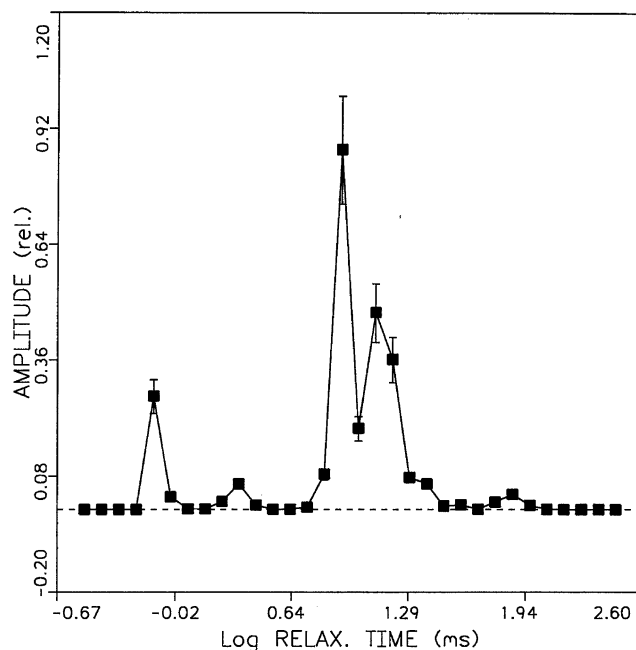


Figure 4. Transverse magnetization decay inversion yielding an NMR T_2 spectrum in a sample of 60% aqueous content. The principal components occur at -0.16 (0.7 ms), leathery network, and between 0.8 and 1.2 (6–20 ms), broad peak encompassing a variety of populations from swelled network and adsorbed surfactant at shorter T_2 's (left side of peak) to surfactant micelles (center and right side of peak) to free water (rightmost portion of peak and small peak at 1.9 (80 ms)).

shown below. Whereas FPD projects information mainly about the smallest diameters of the pores, PGSE tends to reflect their longest dimensions; a significant difference is an indication of a substantial geometrical aspect ratio of the porosities, demonstrating the existence of channels and connections between cavities.

It should be noted that not all of the water present in the samples is seen by the FPD measurements. Tightly bound water is invisible to the DSC in the temperature range used for our FPD measurements. Tightly bound water and the swelled networks containing it undergo transitions at temperatures as low as ~ 180 K.^{37,38} These transitions will be missed by our measurements, and no accounting for the bound water appears in the FPD results, since the DSC data are from temperatures from 233 to 277 K. In PHEMA networks, up to 30 wt % water was found to be tightly bound, and while our PMMA/PHEMA network should be more hydrophobic, there may be similar amounts of tightly bound water present. However, since this water does not influence the DSC signal in our temperature range, it will not adversely influence the FPD results.

NMR Relaxation and PGSE Diffusion. Transverse NMR relaxation measurements were conducted for several specimens, using the principal echo pulse sequence. In each case, the magnetization decay was nonexponential with a broad distribution of rates. A representative T_2 spectrum, obtained by inversion of the magnetization decay data using a recent extension to our relaxation data reduction code,³⁹ is shown in Figure 4. A separate search, conducted with solid-echo techniques, failed to detect rigid

(37) Smyth, G.; Quinn, F. X.; McBrierty, V. J. *Macromolecules* **1988**, *21*, 3198–3204.

(38) Quinn, F. X.; McBrierty, V. J.; Wilson, A. C.; Friends, G. D. *Macromolecules* **1990**, *23*, 4576–4581.

(39) von Meerwall, E.; Thompson, D. *Comput. Phys. Commun.* **1984**, *31*, 385.

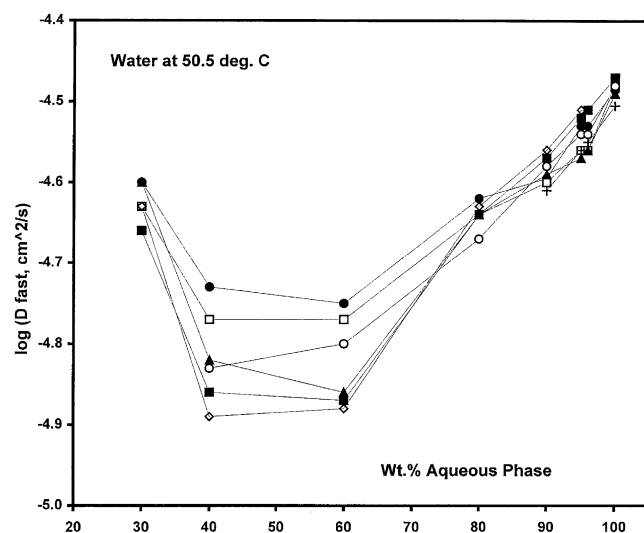


Figure 5. Concentration dependence of diffusion of water molecules in the bicontinuous nanoporous samples at various diffusion times: 8 ms (●); 12 and 15 ms (□); 25 and 30 ms (▲); 100 ms (◇); 200 ms (■); 400 ms (○); and 1000 ms (+). Values for duplicate samples, and duplicate measurements on the same samples, are shown averaged. Uncertainties of ± 0.025 are suppressed to avoid clutter. Values at 30 wt % are thought to be anomalously high due to concentration inhomogeneities (see text). Apparent reversals in the monotonicity between 50% and 100% aqueous content are within the error limits and should not be regarded as significant.

or tightly bound protonic matter. The fastest-relaxing component having significant intensity occurs near 0.7 ms and must be attributed to the glassy network. This relatively high value attests to the considerable molecular mobility of that phase, a consequence of the precursor microemulsion nanostructure as well as the small difference between the curing temperature (55 °C) and the temperature of the NMR and PGSE experiment (50.5 °C). The bulk of the specimen has T_2 values between 6 and 20 ms. These are the components visible in the PGSE experiment, where their full attenuability attests to diffusive mobility and identifies them as arising from the liquid phase, that is, free water and dissolved surfactant.

The portion of the T_2 spectrum from the interstitial liquid phase has been broadened and shifted to substantially lower mobilities by the presence of the network: in the simple aqueous solution of surfactant, T_2 peak amplitudes occur between 50 and 100 ms. The spin dephasing due to molecular encounters with walls is routinely used to extract pore surface-to-volume ratios, and hence pore size distributions, from T_2 experiments,⁴⁰ but doing so requires a detailed model of the pore topology not believed quantitatively reliable here. In our experiment a further complication arises from the presence of two distinct mobile molecular species. Thus, no attempt is made here to determine pore sizes and permeabilities from transverse relaxation data.

The PGSE diffusion experiments in most cases yielded two measurable diffusion coefficients differing by 2 orders of magnitude. The higher of these, D_{fast} , arising from free water, is shown as a function of aqueous content in Figure 5 for various diffusion times. The values measured at 30% liquid are thought to be anomalous, indicative of macroscopic concentration inhomogeneity near the lower limit of the two-phase region. Since the PGSE experiment records a T_2 -weighted diffusivity profile, regions of higher water content, having longer T_2 as well as higher D , will

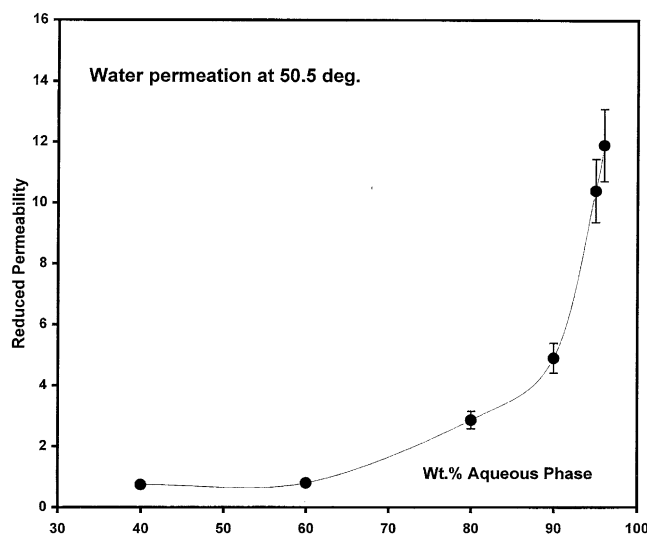


Figure 6. Asymptotic reduced permeability of the bicontinuous nanoporous materials to water containing 10% surfactant, assuming free interstitial diffusion of water.

be more prominent in the recorded average. This hypothesis remains under further investigation. It should be reiterated that in this specimen the echo component from surfactant micelles, while measurable, did not permit the determination of D_{slow} .

The data of Figure 5 display two trends. First, above 40% liquid content, D_{fast} increases monotonically, smoothly approaching the value for the water–surfactant solution in the absence of the glassy network. Second, whereas D_{fast} for above 60% aqueous content is independent of the diffusion time within experimental uncertainty, data at 40% and 60% show evidence of a systematic initial decrease with increasing diffusion time. Both of these trends call for interpretation in terms of restrictions to diffusion.

The first of these trends suggests that the asymptotic permeability of the system increases with increasing aqueous content. Numerical estimates for the reduced permeability may be obtained using eq 2, where D_{∞} at each concentration is the mean of D_{fast} above 100 ms, and D_0 is taken as the value of D_{fast} in a water–surfactant solution containing no network. Implicit in this application of eq 2 is the assumption that the diffusion of water in the liquid phase is free between encounters with network surfaces. The results are shown in Figure 6 and display the expected dramatic concentration dependence. This attribute promises to make bicontinuous nanoporous polymer materials with the present characteristics highly tunable for use, for example, in controlled drug delivery systems.

The relatively modest diffusion-time dependence of D_{fast} , combined with its substantial reduction below D_0 over most of the concentration domain, clearly indicates that, even at our shortest diffusion times, most water molecules have typically undergone multiple encounters with glassy network surface elements. Thus, only an upper limit for the mean free diffusion path, and hence the mean pore size, is available; using eq 3, this value is on the order of 6 μm . This value is comfortably in excess of the mean feature size seen in SEM images in these networks which show features with typical dimensions near 1 μm . On the other hand, the rms diffusion distances for free surfactant-containing water at our highest diffusion times are on the order of 60 μm . As this distance exceeds by large factors not only the PGSE upper limit for the pore size but also the largest structural feature imaged, it is safe to conclude

(40) Kleinberg, R. L. *Magn. Reson. Imaging* **1994**, *12*, 271.

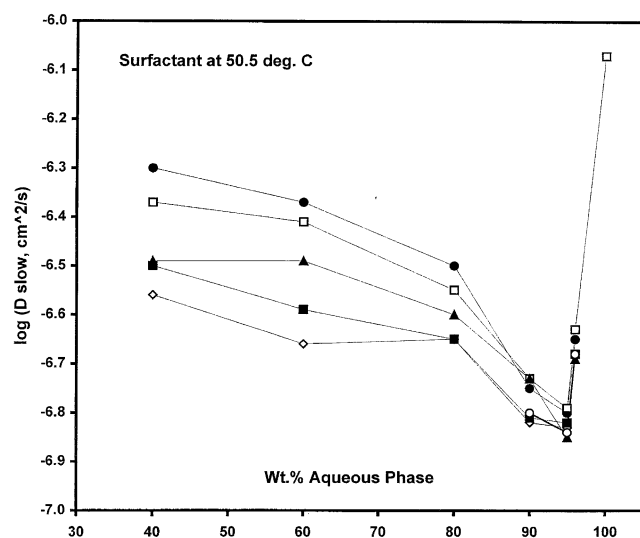


Figure 7. Concentration dependence of diffusion of surfactant molecules in the bicontinuous nanoporous samples at various diffusion times. Symbols are the same as those used in Figure 5; no reliable measurements at 1000 ms were possible. Uncertainties of ± 0.05 are suppressed. Apparent reversals in the monotonicity between 50% and 95% aqueous content are within the error limits and should not be regarded as significant.

that all the networks in the bicontinuous phase are macroscopically permeable to water. This conclusion is easily confirmed by a direct permeation experiment.

Figure 7 shows the concentration dependence of D_{slow} , attributed to surfactant motion, extracted from the same echo attenuation data used to determine time-resolved water diffusion. Several observations are in order. Contrary to the case of water diffusion, surfactant mobility decreases with increasing aqueous content in the bicontinuous region. This decrease is attributed not to a decrease of permeability opposite to the effect observed for water diffusion, but rather to two effects: (1) a tendency for surfactant molecules to undergo rapid surface exchange with the network phase and (2) an increase in the micelle aggregation number as the aqueous content is increased due to an increase in the fraction of surfactant not adsorbed onto the network and hence available for micelle formation. Regarding the first effect, recent literature amply supports this interpretation.^{41,42} Since the observed diffusion coefficient is a time-weighted average of its values for adsorbed and free episodes, and since the network is relatively immobile, the decrease in D_{slow} with increasing aqueous concentration suggests that the surfactant's surface dwell-time fraction increases more rapidly than is compensated for by the expected increase in permeability to dissolved surfactant. Put differently, it appears that as aqueous content increases, surfactant adheres for longer times to less surface area. On the basis of the present experiments, however, it is not possible to separate the effects of surface exchange and permeability on micelle diffusion. The second effect arises because as the aqueous content increases, the fraction of surfactant present at the interface decreases, since the ratio of network surface to pore volume is decreasing. This results in an increase in the concentration of surfactant in the pore space and hence an increase in the aggregation number, and hence size, of the micelles in the pore space. The increase in micelle size and aggregation number has been studied by numerous

researchers, though not in a restricted environment; see, for example, ref 43.

The second observation is the sharp increase of D_{slow} above 95% liquid content. Contrary to the case of water diffusion, for which the small amount of remaining network is no longer a significant impediment and thus differences in network fraction are largely irrelevant, surfactant molecules are sensitive to the loss of adsorbing network surface and perhaps to the disappearance of a laboratory-fixed network. The bicontinuous phase boundary is known to lie between 95 and 96%; our 95% specimen appears distinctly milky, whereas the 96% sample is hazy but nearly transparent.

Third, the explicit time dependence of D_{slow} is much more pronounced than that of D_{fast} , and it persists to a larger concentration of the aqueous phase. Such an observation is expected on the basis of eq 3: since D_{slow} is 2 orders of magnitude lower than D_{fast} , the measurable value of pore size should decrease by 1 order of magnitude, to approximately $0.8 \mu\text{m}$. Indeed, below 80% liquid content, $D_{\text{slow}}(t)$ over the range of diffusion times spans a factor near 2, suggesting that the present experiment may in fact be detecting a significant portion of the transition from short-range free motion of surfactant micelles to partially restricted motion. Unfortunately, this effect is obscured by the effects of surface exchange. Still, since the time scale of PGSE is very much longer than that of surface exchange, the latter cannot be responsible for an explicit time dependence of D_{slow} . Thus, the presence of a significant time dependence at 40%, 60%, and 80% liquid content, and its disappearance by 90%, indicates that within this concentration region the pore size increases from below approximately $0.8 \mu\text{m}$ to above that value. This conclusion is in excellent agreement with the SEM and FPD results.

Further information of interest may be obtained by examining the fraction F_{fast} of the echo intensity arising from the fast-diffusing component. This quantity was found to be significantly dependent on the diffusion time, in a manner qualitatively expected on the basis of differential T_2 -weighting favoring the fastest-diffusing, and hence, presumably, most slowly relaxing, components. In fact, F_{fast} was generally found to increase with increasing τ , τ_1 , and/or τ_2 . One would expect that at the shortest echo times differential weighting effects would be at a minimum and F_{fast} would approach—from above—the proton fraction of the water–surfactant solution. Figure 8 displays F_{fast} recorded at τ between 12 and 20 ms, and shows that this expectation is met at and above 90% aqueous content but fails at lower aqueous content, in a direction opposite to what is expected from the remaining differences in T_2 -weighting. This effect, while not quantitatively understood, attests to the complexity of the interaction between the components of the liquid phase and the surface of the glassy network. Since the network signal itself is not included in the PGSE spin–echo, it appears that surface interactions accelerate water spin relaxation to a greater extent than relaxation of surfactant. But since in each of our PGSE experiments the only parameter varied is the gradient pulse length ($\delta \ll \tau$) without other changes in timing, our results for D_{fast} and D_{slow} should not be affected.

IV. Summary and Conclusions

The following points may serve to summarize the results of this work.

(1) Bicontinuous nanoporous materials were prepared, consisting of a polymeric glassy open-pore phase based on

(41) Tallarek, U.; van Dusschoten, D.; Van As, H.; Bayer, E.; Guiochon, G. *J. Phys. Chem. B* **1998**, *102*, 3486.

(42) Pan, R.; Green, J.; Maldarelli, C. *J. Colloid Interface Sci.* **1998**, *205*, 213.

(43) Chang, N. J.; Kaler, E. W. *J. Phys. Chem.* **1985**, *89*, 2996–3000.

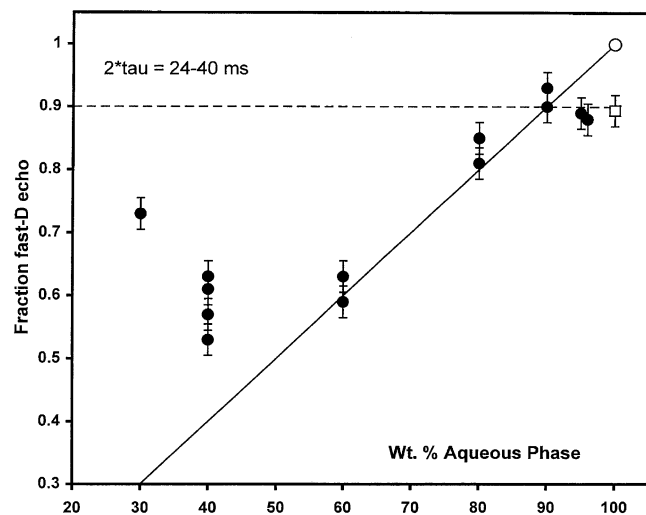


Figure 8. Fraction F_{fast} of the spin-echo for τ between 12 and 20 ms arising from water diffusion, as a function of aqueous content. Symbols include data for duplicate samples and duplicate measurements. The open square (\square) refers to a simple surfactant aqueous solution; the open circle (\circ) indicates single $D = D_{\text{fast}}$ in neat water. The dashed line denotes the fast-diffusing proton fraction expected in the absence of T_2 -weighting; the solid line indicates the network proton fraction.

an MMA/HEMA network and interstitial water containing SDS as surfactant. Eleven samples covered the full bicontinuous range between 30% and 95–96% aqueous content.

(2) Transverse NMR relaxation measurements at 50.5 °C, only 5 °C below the curing temperature, revealed a locally relatively mobile glassy phase. The mobilities seen in the liquid phase are reduced from their values in the absence of network, more strongly for water than for surfactant.

(3) Time-resolved PGSE diffusion measurements between 8 and 1000 ms show two components differing in D by 2 orders of magnitude, attributable to water and surfactant micelles, respectively. Their intensities and D vary systematically with aqueous content and more weakly with diffusion time.

(4) In the bicontinuous two-phase region water diffusion accelerates with increasing aqueous content as a result of increasing long-range network permeability. The reduced permeability to water increases from 0.7 to 12 over the bicontinuous phase domain. The variation of the water diffusivity reflects the decrease in pore size and increase in pore space tortuosity as the aqueous content of the nanoporous materials is reduced. The variation of the surfactant micelle diffusivity reflects a reduction in the micelle aggregation number and possibly a reduction in the local viscosity seen by the micelles in the pore space as the aqueous content of the nanoporous materials is reduced.

(5) Both water and surfactant diffusion rates tend to decrease with increasing diffusion time. This effect is confined to samples with lower aqueous content and is most pronounced at the shortest diffusion times, evidencing restrictions to diffusion. A mean open pore size near 1 μm is derivable from our data near the middle of the bicontinuous concentration domain, consistent with evidence from other types of experiment.

The overall picture that emerges from this work is of a polymer network which has a substantial fraction that is much looser than expected for a swollen glassy phase. This network borders a substantial pore space which increases in volume as the aqueous content is increased

across the bicontinuous domain. This network contains tightly bound water which was not visible to our measurements, possibly ranging to nearly 30 wt % of the samples. The pore space contains the remaining water and surfactant, most of it either adsorbed to the polymer network or as micelles, with a small amount, corresponding roughly to the critical micelle concentration, as dissolved surfactant.

Focusing on the water, we find it present in three forms:

(1) Free water, in pores large enough so that T_2 is much longer than 10 ms, and thus short-time D must be essentially that of water (in solution with 10% surfactant). Then the reduction in D as diffusion time increases should tell us about the size of these larger pores, as we show. Our diffusion time in the composites never gets short enough for us to see free behavior, which is why we only get upper limits for pore size. Our reduced permeability numbers are based on the longest-time D measurements, where the rms diffusion distance is comfortably greater than the largest pores; this lets us assert that the composite is macroscopically permeable.

And (2) water which invades and swells the network molecular structure, and (3) water immobilized in the small pores. Both of these will have T_2 shorter than 10–20 ms, so that our PGSE experiment will not see them. The diffusion coefficient of these species will be much lower or approach zero, but since our PGSE echo attenuation is essentially complete, we know that we cannot be seeing significant amounts of absorbed and trapped water (or immobilized species of any sort).

Focusing on the surfactant, we find it present in three forms also:

(1) Surfactant micelles in free water, clearly visible in the PGSE work as a separate and monodisperse species. Thus, their T_2 should be longer than 10 ms, probably near the right edge of the central peak in Figure 4. It seems apparent that the size of the micelles varies with the aqueous content, increasing as the aqueous content is increased. As discussed earlier, this is likely a surfactant concentration effect with the fraction of surfactant available in the pore space increasing as the aqueous content is increased.

(2) Surfactant adsorbed on network surfaces, or trapped in the network during polymerization. These species will have shortish T_2 , probably at the lower end of the central peak in Figure 4. We see no very slow D component from this species (see above). We cannot hope to distinguish these two populations with our NMR and PGSE experiments.

And (3) dissolved, unassociated surfactant present in a very small concentration in the pore space. Because of its small concentration, this dissolved surfactant is not observed by our experiments.

Focusing on the polymer network: Part of this population is seen in Figure 4 as the shortest T_2 component. But since the intensity of that peak is lower than that expected on the basis of the known composition, the more highly swelled, more mobile, portions of the network must make up part of the central peak also. (This bimodality is, thus, real, and swelled network and relatively unswelled network are somehow distinct.) Remarkably, even the least mobile fraction is relatively loose: 0.7 ms for T_2 is much longer than the 0.02 ms expected for a rigid lattice or a glass. Thus, the network is more leathery than glassy, as we point out. It needs to be remembered that the network is not swollen after polymerization, but rather is born swollen.

The present work demonstrates that the combination of transverse NMR relaxation and time-resolved multi-

component PGSE diffusion measurements is highly effective in characterizing bicontinuous networks for both morphological and kinetic attributes. These results effectively confirm, complement, and extend the information obtained from the bulk and imaging techniques applicable to such systems.

Moreover, this work confirms the understanding that bicontinuous nanoporous polymer materials are excellent candidate systems for applications where mechanical rigidity and erosion-resistance are to be combined with macroscopic permeability to a liquid phase. A principal

example involves implantation or injection in the body to provide long-term controlled drug delivery.

Further work on the characterization of advanced bicontinuous nanoporous materials, with particular concentration on network surface functionalization and release kinetics, is in progress in this laboratory.

Acknowledgment. Two of the authors (K.K. and E.v.M.) wish to thank the Ohio Board of Regents for their support of this work.

LA0264825